Review of Scientific Instruments ARTICLE scitation.org/journal/rsi

Probing the solid–liquid interface with tender x rays: A new ambient-pressure x-ray photoelectron spectroscopy endstation at the Swiss Light Source

Cite as: Rev. Sci. Instrum. 91, 023103 (2020); doi: 10.1063/1.5128600
Submitted: 23 September 2019 • Accepted: 22 January 2020 •
Published Online: 13 February 2020

Zbynek Novotny,[1,2,a)] Dino Aegerter,[2] Nicolò Comini,[1] Benjamin Tobler,[1] Luca Artiglia,[2] Urs Maier,[3] Thomas Moehl,[4] Emiliana Fabbri,[2] Thomas Huthwelker,[2] Thomas J. Schmidt,[2] Markus Ammann,[2] Jeroen A. van Bokhoven,[2,5] Jörg Raabe,[2] and Jürg Osterwalder[1,b)]

AFFILIATIONS

[1] Physik-Institut, Universität Zürich, CH-8057 Zürich, Switzerland
[2] Paul Scherrer Institut, CH-5232 Villigen-PSI, Switzerland
[3] Ferrovac GmbH, Thurgauerstrasse 72, 8050 Zürich, Switzerland
[4] Department of Chemistry, Universität Zürich, CH-8057 Zürich, Switzerland
[5] Institute for Chemical and Bioengineering, ETH Zurich, CH-8093 Zürich, Switzerland

[a)] **Author to whom correspondence should be addressed:** zbynek.novotny@psi.ch
[b)] osterwal@physik.uzh.ch

ABSTRACT

A new endstation to perform *operando* chemical analysis at solid–liquid interfaces by means of ambient pressure x-ray photoelectron spectroscopy (APXPS) is presented. The endstation is located at the Swiss Light Source and can be attached to the soft x-ray *in situ* spectroscopy beamline (X07DB) for solid–gas type experiments and to a tender x-ray beamline (PHOENIX I) for solid–liquid interface experiments. The setup consists of three interconnected ultrahigh vacuum chambers: one for sample preparation using surface science techniques, the analysis chamber for APXPS experiments, and an entry-lock chamber for sample transfer across the two pressure regimes. The APXPS chamber is designed to study solid–liquid interfaces stabilized by the dip and pull method. Using a three-electrode setup, the potential difference across the solid-electrolyte interface can be controlled, as is demonstrated here using an Ir(001) electrode dipped and pulled from a 0.1M KOH electrolyte. The new endstation is successfully commissioned and will offer unique opportunities for fundamental studies of phenomena that take place at solid–liquid interfaces and that are relevant for fields such as electrochemistry, photochemistry, or biochemistry, to name a few.

I. INTRODUCTION

Many important chemical and biological processes occur at the interface between a solid and a liquid. While solid–gas interfaces have been studied widely and in great detail over several decades by using a plethora of surface science techniques, the solid–liquid interface has been much less amenable to these methods. The main reason is that many surface sensitive techniques are electron-based, such as, e.g., x-ray photoelectron spectroscopy (XPS). The very same feature that renders this method surface sensitive, i.e., the large inelastic scattering cross section of electrons in condensed matter, makes it very difficult to collect meaningful signals from a buried solid–liquid interface.

Continuous efforts over the last two decades driven by the groups at the Advanced Light Source (ALS) and BESSY II led to the development of commercially available, differentially pumped hemispherical energy analyzers for ambient-pressure XPS (APXPS).[1–7] Such analyzers allow operation at pressures in the order of a few

tens of mbar and can thus tolerate the vapor pressure of around room temperature water, a prerequisite for the study of interfaces involving liquid water.[8–12] Historically, there were several different approaches used to study liquid–solid interfaces using x rays. Most of the effort centered on building compact cells that were placed within a vacuum apparatus. Such cells use either a photon-transparent membrane, such as silicon nitride or graphene, that allows us to operate such cells in vacuum, or they use a proton transparent membrane that allows a slow diffusion of the electrolyte from the cell to the chamber where the material of interest, deposited on the outer side of the membrane, can be studied.[13,14] These cells can be equipped with a reference and counter electrode (CE), and also allow a continuous flow of a fresh electrolyte and removal of the gas-phase products. Since the electrolyte is contained within the cell, even corrosive electrolytes can be used without risk of damage to the instrument and the pressure within the cell can be much higher (<100 mbar) than would be otherwise compatible with APXPS analyzers or the use of soft x rays. Probably, the largest disadvantage of such cells is the type of samples that can be used since the sample of investigation is deposited on the membrane and has to be designed in parallel with the design of the cell. Some samples, such as well-defined single-crystalline systems, are not compatible with the cell approach. Another approach to study solid–liquid interfaces uses a so-called offset droplet method.[8] Here, a thin capillary forms a droplet on a surface,[15] and by balancing the flow of water (to compensate the evaporation rate due to the pumping via the orifice of the electron analyzer), a droplet of a constant volume can be maintained over an extended period of time. While this approach can work with any sample (as long as the optical axis of the electron spectrometer is vertical), the use of the offset droplet technique is likely to be difficult to use for electrochemical measurements because of the evaporation effects, which will make the control of the electrolyte concentration very difficult. The evaporation might also result in significant contamination issues since the evaporating electrolyte will likely leave any carbon contamination behind, which will build up within the volume of the droplet over time. Another type of the electrochemical cell is being developed by the group in Lund[16] that will allow *ex situ* characterization of electrochemically studied electrodes with a very short transfer time between the electrochemical and XPS measurements.

A particularly attractive setup for APXPS studies at solid–liquid interfaces has recently been presented by Axnanda *et al.* in Ref. 17. This endstation is installed at the Beamline 9.3.1 of the ALS and uses a commercial APXPS analyzer combined with a relatively simple analysis chamber (AC) that can operate at pressures of up to some 30 mbar. Inside this chamber, a beaker with an aqueous electrolyte solution can be placed below the entrance cone of the analyzer. The sample can be configured in a standard three-electrode setup for *in situ* cyclic voltammetry when dipped into the electrolyte. Well-defined surface preparations can be achieved by electrochemical means, using appropriate reduction–oxidation cycles, leading to atomically clean surfaces. The sample can subsequently be moved in front of the analyzer cone, a short distance from the tiny entrance orifice. In the case of hydrophilic surfaces, a continuous water film of a few tens of nanometers thickness can be maintained by adjusting the water vapor pressure.[17–23] While the solid sample still needs to be grounded for proper energy reference, the electrochemical potential within the liquid, and thus, the characteristics of the Helmholtz layer at the interface, can be controlled relative to the reference electrode (RE).[17–23] While this thin film approach has certain limitations since the ion mass transport along the film direction is limited,[20] it was selected as the most promising since it can be used with a wide range of samples, including single crystals, as presented in this manuscript.

Inspired by the original design of the endstation at Beamline 9.3.1 at the ALS,[17,20] we built a new custom-made APXPS endstation combining tender x-ray photoemission with *in situ* electrochemistry. The endstation was designed and assembled by Ferrovac GmbH. Compared to the endstation at Beamline 9.3.1 and other dip and pull-capable endstations currently being built at BESSY II and MAX IV, this new setup is more complex and features a preparation chamber (PC) with capabilities for sample preparation under ultra-high vacuum (UHV) conditions, offering ion etching, annealing, molecular beam epitaxy, etc., as well as sample characterization with low-energy electron diffraction (LEED) and Auger electron spectroscopy (AES). By these means, it will allow the preparation of well-defined single-crystalline samples, e.g., for studies of model catalysts under *operando* conditions. The endstation is mobile and can be used either at the PHOENIX I beamline with tender x rays for dip and pull experiments on solid–liquid interfaces, or at the *in situ* spectroscopy beamline (X07DB) with soft x rays for solid–gas type studies.

In Sec. II, the description of this new endstation, internally named as Solid–Liquid Interface Chamber (SLIC), is intentionally very detailed; this is motivated by the fact that the endstation was built with a goal to serve as a tool for an interested user community, and therefore, we want to provide enough details to potential future users of this instrument. The SLIC is a third APXPS endstation available at the Swiss Light Source (SLS) and shares the same electron analyzer as the existing solid–gas interface chamber[24] and the liquid jet chamber.[12]

II. EXPERIMENTAL SETUP

A. General concept of the endstation

The experimental endstation consists of three interconnected UHV chambers made from 304L stainless steel: one for the preparation of well-defined surfaces and interfaces using surface science techniques, one for the APXPS experiments, and one for sample transfer across the two pressure regimes that can also be used as a fast entry load lock (see computer-generated rendering of the whole instrument shown in Fig. 1). The transfer chamber is connected to the preparation chamber (PC) via edge-welded bellows to provide some degree of freedom for movement between the two chambers. Sample transfer between the chambers is possible by a combination of wobble sticks and magnetically coupled transfer arms.

The endstation (shaded in blue in Fig. 1) is connected to a Scienta HiPP-2 APXPS analyzer that is mounted on its own frame (rendered in gray color in Fig. 1). It is modular and can be attached to the analyzer with or without the PC. Both, the PC and analysis chamber (AC) have their own supporting frame made from aluminum profiles (Kanya AG) and both of these frames rest on rotatable wheels equipped with jacks that allow lifting of the wheels by ~5 mm from the resting position. The frame of the PC allows height adjustment,

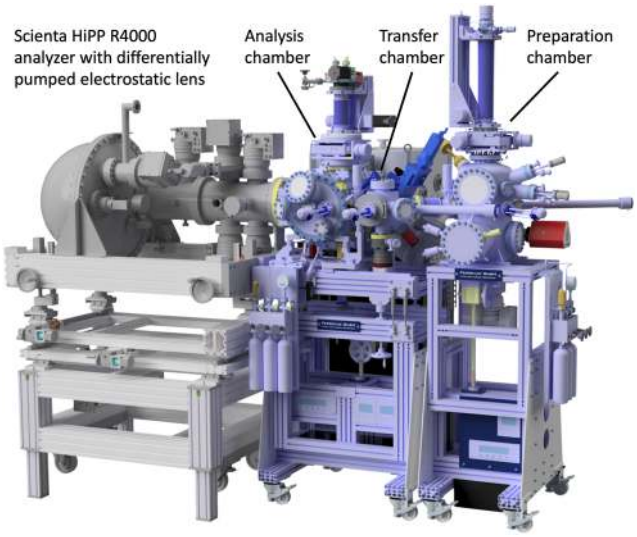

FIG. 1. Computer-aided design (CAD) rendering of the new endstation for ambient pressure XPS at solid–liquid interfaces. The left part of the instrument (gray shaded) is a Scienta R4000 HiPP-2 electron analyzer that was already existing at the SLS.[12,24] The right part (blue shaded) shows the new three-chamber endstation.

while the frame of the AC allows for fine adjustments of both the height and tilt via four independent gimbals. This is required for the connection of the AC frame to the frame of the APXPS analyzer. Once the frames are connected (via three M14 bolts), the AC chamber and the load lock can be moved sideways to/from the analyzer nose cone using linear side rails. When this side movement is not desired, a locking mechanism preventing this linear movement must always be engaged.

The setup of the Scienta R4000 HiPP-2 electron spectrometer is described in detail in Refs. 12 and 24. The front of the electrostatic lens system is fitted with titanium cones with varying entrance apertures. For the solid–liquid interface experiments with water vapor pressures up to 30 mbar, a cone with an aperture diameter of 300 μm and a working distance of 600 μm is used. The analyzer frame allows movement along six degrees of freedom: in-plane horizontal movement (X and Y direction), in-plane rotation (WXY) and height (Z) adjustment by three independent stepper motors (Z_1, Z_2, Z_3) that can be used to adjust both height as well as tilt of the entire setup up to about 10° in any direction. Movement along each of these axes is done via stepper motors, with optical encoders determining the actual positions. For a successful alignment of the endstation to the synchrotron beamline, the optical axis of the synchrotron light beam and the optical axis of the electron spectrometer need to be aligned within about 100 μm of the working distance of the electron analyzer.

Once the analysis chamber is attached to the analyzer, the upper part of the frame of the AC is decoupled from its lower part and the entire setup (AC chamber and the analyzer) rests on the tripod (Z_1, Z_2, Z_3) of the analyzer. Since the AC chamber is rather heavy, the weight load imposed onto the electron analyzer is compensated by four high-pressure gas springs.

The actual alignment procedure is performed via a computer-controlled positioning system of the analyzer frame using a set of two scintillating crystals: cerium-doped yttrium aluminum garnet (YAG:Ce) on a removable sample plate placed on the sample manipulator (10 × 10 mm^2) and an additional circular cerium-doped lutetium aluminum garnet (LuAG:Ce) crystal with 20 mm diameter that is glued to a viewport located on a flange that is intersecting the optical axis of the synchrotron light. The latter crystal is mounted permanently and can be used to quickly check the position of the beam during experiments. The initial alignment consists of an approximate positioning of the beam spot and its visual comparison with respect to the aperture of the titanium cone. Once the beam is aligned within ~500 μm accuracy, the sample plate with the YAG:Ce crystal is replaced by a polycrystalline Au sample. The fine alignment of the beam is performed by using a de-focused beam and by maximizing the count rate reading on the detector of the electron spectrometer using the intensity of the Au 4f core level peak measured in a snapshot mode. The alignment procedure requires the optimization of the lateral position of the beamline entry window assembly (see Sec. II B), the position of the analyzer frame (optimizing the working distance), beam focusing, and the position of the manipulator and has to be performed iteratively. This procedure can be accomplished within less than an hour with previous experience once the endstation is placed to a position marked on the floor and attached to the beamline.

For safe transport of the endstation when the frame is placed on wheels, additional steel plates with a total weight of 100 kg have been fixed to the bottom parts of the frames of both PC and AC, with the aim to lower the center of mass of the entire assembly. To further increase the stability of the endstation during transport, the orientation of two out of four wheels can be fixed with a dedicated profile that is attached to the side plates of the frame. These side plates are installed to increase the overall stiffness of the frame and are attached to the frame by several screws that need to be loosened when the height of the frame needs to be changed. The endstation is designed to fit into an experimental hutch with a ceiling height of 2600 mm, and during transport, it can be lowered to pass through doors with a height of 2000 mm. Figure 2 shows the complete endstation fitted inside the hutch of the PHOENIX I beamline of the SLS.

B. Light sources

The endstation is designed to operate at two different beamlines at the SLS: PHOENIX I and X07DB. Since the incident radiation is typically linearly polarized, a 90° geometry between the incident synchrotron light and the optical axis of the electron spectrometer was chosen for both beamlines. By using this geometry, the angle between the polarization vector and the electron detection axis can be varied between 0° and 90° at the PHOENIX I beamline,[24] and the same geometry was used at the X07DB beamline.

PHOENIX I is an undulator beamline with a photon energy range of 0.8–8.0 keV. This beamline uses an elliptical APPLE II undulator, with a photon flux of 5 × 10^{11} photons/s at 4 keV, an energy resolution of 1 × 10^{-4} and beam focusing using Kirkpatrick-Baez (K-B) mirror optics from 2 × 2 mm^2 down to 2.5 × 2.5 μm^2.

For experiments with soft x-ray excitation, the *in situ* spectroscopy beamline (X07DB) can be used, which is a bending magnet

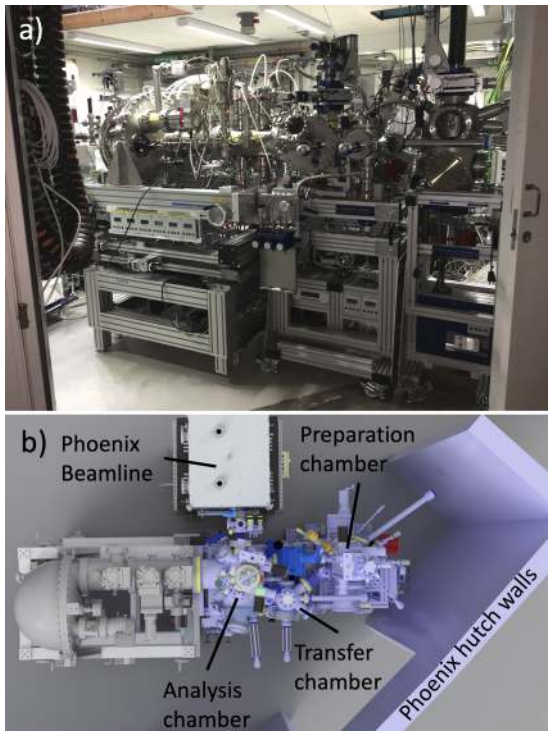

FIG. 2. (a) Photograph of the solid–liquid interface chamber (SLIC) attached to the PHOENIX I beamline. (b) 3D CAD model showing the top view of the endstation inside the PHOENIX I beamline [here, only the Kirkpatrick-Baez (K-B) focusing mirror chamber is shown] with a highlighted position of the lead hutch walls and the beamline.

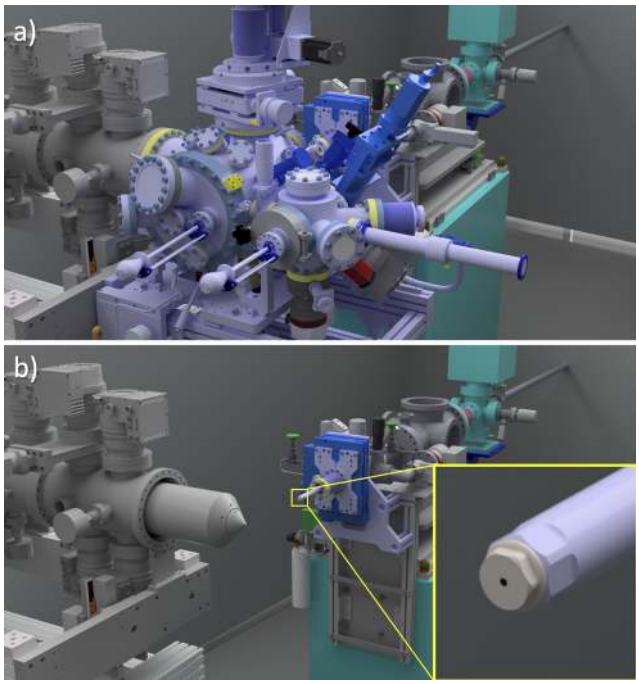

FIG. 3. Beamline adaptation—silicon nitride membrane beamline entry-window assembly with (a) and without (b) the AC chamber and transfer chamber shown. The inset in panel (b) shows a zoomed-in view of the replaceable nut (shown in gray color) that is used to support the silicon nitride window membrane (not shown in rendered image), which is attached to an aluminum tube (shown in blue color).

beamline. It offers photons in the energy range between 270-1800 eV with a spectral resolution >3000. The design and parameters of the X07DB beamline are nearly identical to the PolLux beamline, which is described in detail in Ref. 25.

To connect the APXPS endstation to these beamlines, a dedicated beam entry and alignment assembly was designed for each of them. Figure 3 shows how the silicon nitride window for the X07DB beamline is mounted on a two-axis manipulator for beam alignment. It separates the UHV side of the beamline from the ambient-pressure environment inside the AC. A replaceable aluminum tube can be screwed to this two axis-manipulator and is sealed by a Viton™ O-ring. At the end of this tube, a threaded nut, again sealed by an O-ring, is used to support a silicon nitride membrane window that is glued to the nut [inset of Fig. 3(b)]. Two different types of membranes were used for the different photon energy ranges. For the X07DB soft x-ray beamline, a membrane of 0.5×0.5 mm^2 area and thickness of 75 nm is used (Silson Ref.: 11006128). For the PHOENIX I tender x-ray beamline, the area is 1.5×1.5 mm^2, and the thickness is 500 nm (Silson Ref.: 11608127).

The beamline entry alignment assembly for the PHOENIX I beamline is almost identical but has the additional option for a vertical tilt of the aluminum tube. For radiation safety, a Pirani gauge is part of this assembly and is used as an interlock for the tender x-ray beamline. The beamline shutter valves are closed automatically when the pressure in the AC chamber exceeds 40 mbar. This is used to avoid tender x-ray exposure to the user when the AC chamber is vented and accessed through the front door flange [see Fig. 4(b)]. An additional interlock is installed to the AC door flange that ensures that the door flange is closed when the beamline valves are open.

C. Pumps and pressure measurement

The base pressure in the AC is below 1×10^{-10} mbar. This value was obtained after the first commissioning beamtime experiments with electrolytes inside the chamber, following a prolonged bakeout at 150 °C. The base pressure of the baked preparation chamber (at 130 °C) is 1.5×10^{-10} mbar and the transfer chamber has a base pressure of 1×10^{-8} mbar (unbaked). The pressures in the PC and the AC are measured by compact cold cathode gauges (Pfeiffer IKR 270). In addition, the AC chamber is equipped with a combined Pirani/capacitance gauge (Pfeiffer PCR 280) to cover the pressure range needed for ambient-pressure experiments (5×10^{-4} mbar to 1000 mbar). The pressure in the transfer chamber is measured with a full-pressure range gauge (Pfeiffer PKR 361).

For experiments using liquid water, the first stage of the electron analyzer is pumped with two turbomolecular pumps (Pfeiffer HiPace 300) backed with a shared roots pump (Adixen ACP28) with the gas ballast (GB) fully open. This configuration was used to perform experiments at 25 mbar of water vapor over an extended period (one week) when using a standard Scienta titanium cone with an

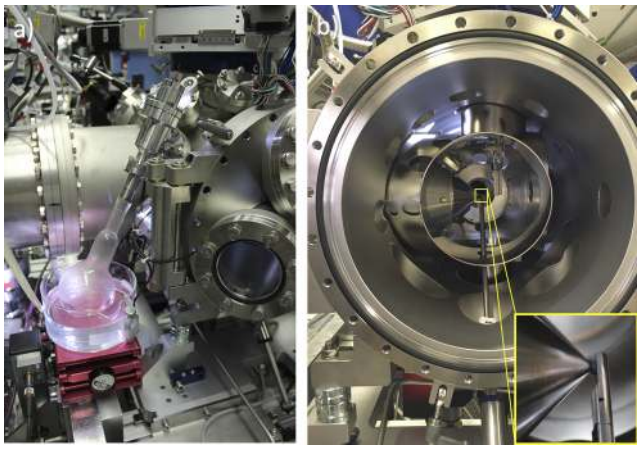

FIG. 4. (a) External water reservoir with a glass-to-metal adapter for a fast pressure equilibration of the water vapor inside the AC. (b) View inside the vented AC chamber through the door flange. The picture shows the AC chamber with the μ-metal shield installed, of which a front panel has been removed for easy access to the sample area. The inset in (b) shows the lid with a flat rubber seal (Viton) that can be pressed (via a wobble stick) against the entrance cone of the HiPP-2 analyzer before the AC chamber is vented while the analyzer is kept under vacuum.

aperture of 300 μm, with pressure in the 10^{-4} mbar range in the prelens stage and 10^{-6} mbar range in the second, differentially pumped stage, respectively.

Both, the PC and the AC are pumped using turbomolecular pumps (Pfeiffer HiPace 700), and the transfer chamber (load-lock) is pumped with a HiPace 80 turbomolecular pump backed with a membrane pump. All three turbomolecular pumps can be separated from the respective chamber via a gate valve. Roots pump from Adixen ACP28 G CV is used as backing pre-vacuum pump for the AC. This pump is designed to pump condensable vapors (CV option) as well as corrosive gasses (G option). The backing pump for the PC is an Adixen ACP15 roots pump with the GB closed.

During experiments with liquids and electrolytes, the gate valve in the AC is always closed to protect the inner part of the turbomolecular pump, as well as to avoid contamination from the oil used for the bearing lubrication within the turbomolecular pump. After finishing experiments with liquids/electrolytes, special care has to be taken when pumping the AC back to UHV. We achieve this by using the Adixen ACP28 G CV (GB open) backing pump connected directly to the AC chamber via a needle valve. This is mainly owed to water condensation at the cold parts of the chamber, such as bellows, where the water could freeze, forming ice and causing possible damage. Since water is expected not to freeze at pressures above 6 mbar, the chamber is pumped slowly, leaving the total pressure between 7-10 mbar by adjusting the pumping speed via the needle valve. Once all the liquid water is pumped away, the gate valve between the AC and the HiPace 700 pump is opened and the turbomolecular pump is restarted.

D. Analysis chamber (AC)

The analysis chamber is designed according to UHV standards and allows experiments both under UHV as well as ambient pressures up to some 50 mbar, currently limited by the 300 μm aperture of the electron spectrometer. The analysis chamber is equipped with a 12-in. outer diameter door flange that can be equipped with an O-ring seal made of Viton for quick access during APXPS experiments or can be fitted with a standard copper gasket when the AC is operated in the UHV regime. To seal the analyzer entrance aperture while venting the AC, a dedicated lid is installed on a single shaft wobble stick equipped with a port aligner. The lid is made from a flat rubber seal (Viton) that can be pressed against the entrance cone of the HiPP-2 analyzer [see inset in Fig. 4(b)]. This allows venting of the AC to atmospheric pressure while maintaining the vacuum within the electron analyzer.

When the endstation is operated using soft x rays, a μ-metal shield for complete magnetic shielding of the sample environment is used. This magnetic shield consists of a main μ-metal tube and several sleeves and skirts for optimized shielding while having access to the sample region through the sample-facing flanges and viewports [see Figs. 5(a) and 4(b)]. For studies using tender x rays involving electrolytes, the μ-metal shield can be removed such that it is not exposed to potential spillage.

The XYZ sample positioning is realized via a standard manipulator with bellows (Ferrovac Boomerax series). The rotation (R) is done via a differentially pumped rotary platform (DPRF 450, McAllister Technical Services). The manipulator insert is mounted to a DN63CF flange located on top of the rotary platform. This approach allows the development of dedicated manipulator inserts that can be easily exchanged based on the specific experimental needs. Currently, one manipulator insert is available for experiments targeted at the solid–gas and the solid–liquid interfaces (see Sec. II E for details), while designs of other manipulator inserts are currently underway. The movement of the manipulator is fully motorized (XYZR) using 5-phase stepper motors. The absolute

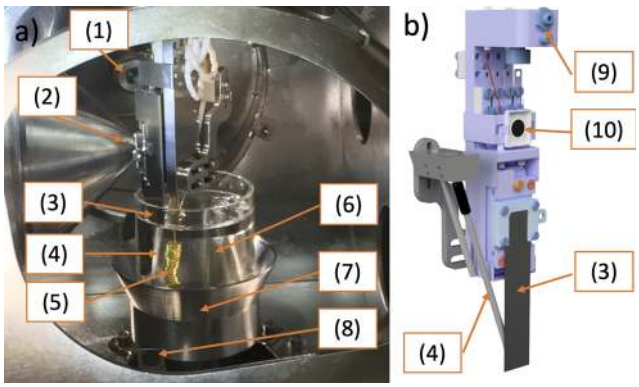

FIG. 5. View inside the analysis chamber showing (a) a photograph and (b) a 3D CAD rendering of the manipulator insert. The relevant components are labeled using numbers: (1) silicon nitride membrane separating the beamline and the APXPS chamber, (2) Ti cone of the electron analyzer, (3) sample (50 × 10 mm^2), configured as a working electrode (WE) (4) reference electrode (RE), (5) counter electrode (CE, here a gold coil), (6) Pyrex beaker with electrolyte (0.1M KOH at 12 mbar), (7) beaker holder with XYZ movement, (8) end-piece of the wobble stick used for capping the Ti cone (2) during venting of the analysis chamber, here in its parking position, (9) adjustment screws to compensate for a variable sample thickness, and (10) photodiode to measure photon flux.

position and rotation in each direction are monitored using optical encoders (Numerik Jena for XYZ, RENISHAW for rotation), with the smallest step of 78 nm for XYZ movement and 262 144 counts per revolution for the rotation encoder. For dip and pull experiments, the motors are operated at a speed of 50 μm/s with 10 s acceleration/deceleration.

The XYZR movement is computer-controlled via an Experimental Physics and Industrial Control System (EPICS) interface. For safety reasons, position limit switches are implemented for the XYZ movements. The sample position can be viewed remotely via an optical camera (uEYE) using light provided by low-power light-emitting diodes with adjustable intensity (VCH-10, Prevac).

For experiments involving solid–liquid interfaces, the AC contains a beaker holder [labeled with No. 7 in Fig. 5(a)] that is placed on an XYZ manipulator with ±7.5 mm XY travel and 100 mm Z travel. The Z travel is currently set manually, but the Z motion will be motorized in the future. The beaker holder is removable and is available from stainless steel or aluminum. The beaker (custom-made) has a round shape with one side flattened that allows closer positioning to the end of the Ti analyzer cone, thus minimizing the distance between the electrolyte level in the beaker and the measurement point. In addition, we use a second, large volume equalizing reservoir placed between the AC door flange and the μ-metal shield (not shown in the picture).

An external equalizing reservoir is attached to the AC,[17,20] connected via an all-metal angle valve (VAT) using VATRING-system sealing technology [see Fig. 4(a)]. This additional liquid reservoir is using a custom-made DN16CF glass-to-metal adapter with a rounded flask attached by a glassblower. This reservoir can be heated up or cooled down to quickly equalize the water vapor pressure within the chamber, allowing to equilibrate the water vapor pressure within a few minutes.

For experiments involving photochemistry or photoelectrochemistry, a sapphire viewport (DUV grade, 99.8% internal UV transmission at 248 nm) is attached to a port directly facing the sample in APXPS measurement position. This viewport is directly used with an artificial sun (LS0400, LOT Quantum Design, equipped with AM1.5-Global filter and electronic shutter). The light is coupled to the chamber via an optical fiber.

Gas dosing can be done either via backfilling of the chamber using an all-metal variable leak valve (VAT, series 59.0) or via a tubular doser aligned along the analyzer entrance cone directly facing the sample. This tubular doser is connected to the same type of VAT leak valve and can be used either for gas dosing or as a gas sniffing nozzle pumped via a gas line connected to the PC for gaseous product analysis via mass spectrometry. It can be brought to close proximity of the sample using a 50 mm Z-shift translator.

The AC is equipped with a gas dosing system designed to host up to three Minican® bottles. The gas lines are made from stainless steel tubing welded to ConFlat (CF) flanges and can be pumped with the turbomolecular pump of the transfer chamber down to its base pressure. The pressure in the gas dosing system is measured with a pulsed Pirani gauge (Pfeiffer TPR 270) and an oil-free, Grade A mechanical pressure gauge (Wika) made from 316L steel, covering a pressure range from −1 bar to 15 bars. When the Minican bottles are properly attached, i.e., the dead volume is pumped before pressing the membrane, the purity of the gas is sufficiently high to perform APXPS experiments when the AC chamber is backfilled to the mbar pressure range.

E. Manipulator for solid–liquid and solid–gas interface experiments

The design of the manipulator for probing solid–liquid interfaces is shown in Fig. 5, where a real picture [(a) back view], as well as a 3D CAD rendering [(b) front view] of the manipulator is displayed. The parts of the manipulator in the vicinity of the sample are produced from titanium. Samples mounted on Omicron-type sample holders [labeled as No. 3 in Figs. 5(a) and 5(b)] can be inserted into a drawer-style receiver [Ferrovac RECOM(Ti)]. The sample receiver is electrically insulated, and the sample can be biased up to a few tens of volts. The sample plate can be heated using a 50 W/cm^2 PBN/PG/PBN heater (Thermic Edge). This heater can bring the sample up to 227 °C. The maximum temperature is limited mainly due to the installed photodiode [Opto Diode, model AXUV20HS1, No. 10 in Fig. 5(b)] that is used to measure the photon flux inside the chamber. The entire end piece of the manipulator can be adjusted for different sample thicknesses (X-offset) so that the sample surface can be in the center of the rotation axis.

For electrochemical measurements, a potentiostat from Bio-Logic Science Instruments (SP-300) equipped with a board for electrochemical impedance spectroscopy and a standard electrometer is available. During APXPS measurements at solid-electrolyte interfaces, the electrode connections within the potentiostat interface (EC-Lab V11.20 software package) are wired such that the WE is grounded. The electrometer is connected to three separate BNC feedthroughs for WE, RE and CE placed in the upper part of the manipulator. Here, the connections are made using short, custom made adapters between the BNCs and the 2 mm banana plugs of the electrometer. Inside the chamber, the wiring is made using silver wires, with the very last parts of wiring (for RE and CE) made using 0.5 mm thick Au wires.

For the solid–liquid interface experiments using the dip and pull method, a standard sample size of 50 × 10 × 1 mm^3 was selected, but other sample geometries with different widths or thicknesses can be accommodated within the existing design. While the sample length is currently standardized to 50 mm, only 25 mm can be dipped into the electrolyte, since the upper half of the sample cannot reach the electrolyte, ensuring that no part of the manipulator should be in contact with the electrolyte.

F. Preparation chamber (PC)

The preparation chamber is designed for sample preparation and characterization under UHV conditions. The manipulator in the PC is nearly identical to that in the analysis chamber. Heating of the sample up to 627 °C can be done on the manipulator by using the same PBN/PG/PBN heater as used in the AC chamber. The temperature is limited due to the installed Pt100 temperature sensor (Innovative Sensor Technology, 600 °C series). For a higher temperature annealing (up to 2000 °C), a dedicated e-beam annealing heater (Ferrovac HSAS40) is available. The manipulator is motorized in the Z direction (height) using a stepper motor (Nanotec), although this stepper motor will be soon replaced with a 5-phase motor that does not produce significant vibrations. The XY travel

(±12.5 mm) is performed manually via a micrometer drive, and rotation between 0-355° is possible. Similar to the manipulator in the AC, the sample can be biased up to tens of volts via a BNC feedthrough. The same feedthrough can be used to measure the sample current during ion bombardment. The samples are transferred using a wobble stick that is capable of reaching the e-beam stage, the manipulator, the sample storage for four samples by using a drawer-style receiver attached to a miniature linear/rotary feedthrough and a magnetically driven single shaft transporter for transport between the PC and the transfer chamber. Up to five samples with a geometry suitable for the dip and pull experiments can be stored in the PC. There are two ion gun sources available: a Specs IQP 10/63 penning type ion source[26] and a VG EX05 focused source equipped with a scanning unit.

Ports for up to four evaporators (DN40CF) facing the same focal point in the center of the chamber are available. The evaporators are near-horizontally mounted facing slightly upward (downwards) by ~5° (~22°), respectively. Currently, one commercial electron-beam evaporator is available (Focus EFM3 single) that can be calibrated using a water-cooled quartz crystal microbalance (Inficon).

The PC is equipped with a quadrupole mass spectrometer (Pfeiffer PrismaPlus QMG220) with a mass range of up to 200 amu. For sample characterization, a combined low-energy electron diffraction (LEED) and Auger electron spectroscopy (AES) instrument is available (OCI, type BDL800IR-MCP2-3GR-100DEG). It is equipped with two microchannel plates for low-current LEED measurements.

The gas dosing system is analogous to the one installed in the AC (see Sec. II E). Currently, the gas lines can be pumped via the turbomolecular pump of the PC when the gate valve is closed. There are two leak valves (VAT, the same model as used in the AC) available in the PC, both connected to the two ion guns. The PC is fully bakeable with a typical bakeout temperature of 130 °C. A bakeout tent is available for a fast bakeout setup.

III. COMMISSIONING: POTENTIAL CONTROL

The first commissioning beamtime at the PHOENIX I beamline was conducted in December 2018, in which the capabilities of this endstation were demonstrated. The experimental procedure is described in detail in the supplementary material. The spectra shown in Fig. 6 demonstrate potential control within a thin electrolyte layer (0.1M KOH) stabilized by the dip and pull method at 12 mbar. The thickness of the water film was determined using formulas (1–5) from Ref. 20, using the calculated inelastic mean-free path (IMFP) value for liquid water from Ref. 27. The thickness of the water film is determined from the Ir 4f core-level peaks measured in high-vacuum (HV, pressure of 4.9×10^{-8} mbar) and at 12 mbar of water vapor after pull from the electrolyte, and assuming a working distance of 600 μm between the sample and the analyzer and considering the electron attenuation both through the liquid water as well as the gas phase. Using this, we determined a thickness of 21 nm for the sample polarized at +1.05 V with respect to the reversible hydrogen electrode (RHE) and 31 nm for sample polarized at +0.05 V vs RHE.

Here, the working electrode [Ir(001) substrate] is grounded such that the Fermi levels of sample and spectrometer are aligned, and hence, the corresponding iridium core level peaks do not shift with the bias applied to the electrolyte. In contrast, the O 1s core-level peaks associated with the liquid (533.2 eV) and gas phase water (535.6 eV) shift proportionally by a factor of ×0.82 to the applied bias. This value is smaller than what would be expected from a complete potential drop within an ultrathin electrochemical double layer. This observation is due to the limited ionic strength of the solution and the very thin electrolyte film and is in good agreement with a proportionality factor reported previously.[22] The binding energy values for liquid and gas phase water peaks given above are for a bias of +1.05 V (black spectra in Fig. 6), since the peak positions are very similar (higher by +0.3 eV) to those from a reference Ir(001) sample measured in 25 mbar of water vapor at ~21 °C

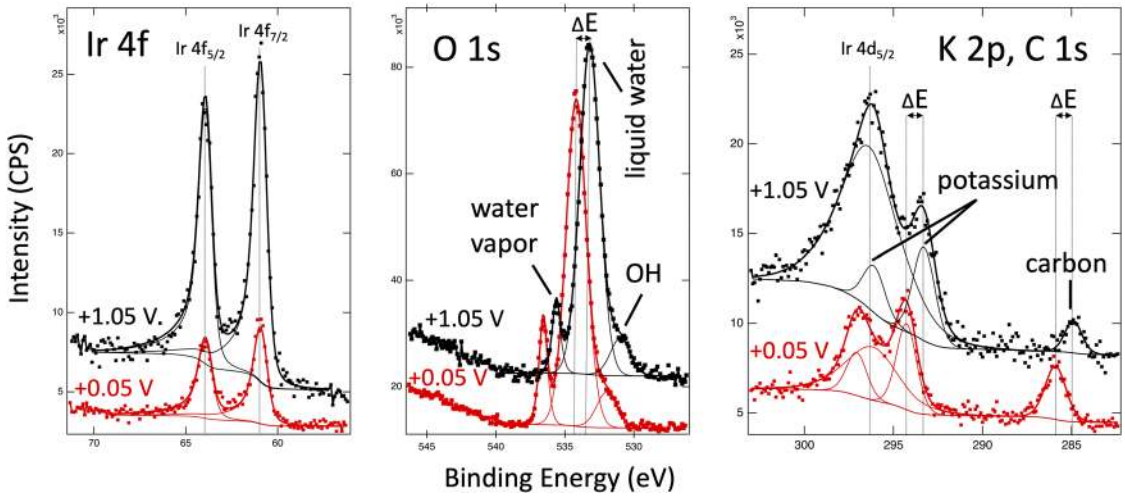

FIG. 6. Ambient pressure XPS spectra acquired after dip and pull cycles with the Ir(001) sample and 0.1M KOH electrolyte at different potentials relative to the RHE scale, as discussed in the text and indicated in the figure. Data recorded at the PHOENIX I beamline at 12 mbar base pressure, using a photon energy of 4000 eV.

(data not shown) that should correspond to adsorbed water. We associate the small shoulder at the low binding energy side of the O 1s spectrum (531 eV at a bias of +1.05 V) with the presence of OH groups in the liquid film (see below).

The power of this method is further illustrated by the K 2p and C 1s signals on the right-hand panel of Fig. 6. The K 2p spin-orbit doublet, which overlaps with the Ir $4d_{5/2}$ signal, clearly shifts with the applied potential, as potassium is part of the electrolyte. The same is true also for the C 1s signal, which is rather interesting. It means that the electrolyte/Ir(001) interface is clean, and the carbon contamination is clearly outside the Helmholtz layer, either within the thin liquid film or at the surface of the liquid.

As shown in Fig. 6, the thin electrolyte layer contains 0.1M of KOH salt and carbon contamination. Since both potassium, hydroxyl groups and carbon move by the same amount with applied bias, we assume a homogeneous distribution of these species within the electrolyte film. In the case of 0.1M KOH, 0.1 mol of KOH are diluted in 1 liter of water—thereof in 55.6 mol of water molecules (M_{H_2O} = 18 g/mol and ρ_{H_2O} = 1000 g/l). The atomic concentration of K or OH to O 1s from the liquid water should show a ratio of 0.1/55.6 for an ideal electrolyte. The measured OH^-/H_2O ratio in the electrolyte is actually much higher than this value: 26 ± 4 times higher for a thick water film stabilized at 25 mbar of water vapor, where the Ir substrate is not visible for 4000 eV photons (data not shown) and even higher for the case of thin films as shown in Fig. 6, where the concentration is higher by a factor of 60. While this could be attributed to beam damage caused by the focused beam from the undulator beamline, we find a near-stoichiometric ratio between potassium ions and hydroxyl groups within a thin electrolyte film (concentration ratio of potassium to hydroxyl groups is 1.23 ± 0.32 both for thin and thick films) as determined from the equation

$$\frac{c_K}{c_{OH}} = \frac{I_{K2p}}{I_{O1s,OH}} \frac{\sigma_{O1s}}{\sigma_{K2p}} \frac{\lambda_W(E(O1s))}{\lambda_W(E(K2p))} \quad (1)$$

for a photon energy of 4000 eV, using cross sections (including angular distribution asymmetry parameters) from Ref. 28 and the calculated inelastic mean-free path values for liquid water (λ_W) from Ref. 27. The possible reason for this higher potassium and hydroxyl concentration could be caused by a local heating/beam induced effects, and/or evaporation of the water from the liquid film due to the pressure gradient in the vicinity of the differentially pumped nozzle of the electron analyzer[29] together with limited diffusion of the ions within the thin electrolyte film. In the case of the ultrathin film, the concentration measured with XPS is about 6M, which is still low enough to be considered a liquid electrolyte since the solubility of KOH in water is around 18.4M at 10 °C.[30–32] This difference in the KOH concentration in bulk electrolyte vs ultrathin film can be explained assuming an electrolyte temperature within the ultra-thin film of 15.4 °C, compared to the temperature of 0.1M KOH in the beaker which was calculated to be 9.7 °C.[32] This assumption can be rationalized by adiabatic cooling of the bulk 0.1M electrolyte in the beaker due to a continuous pumping of the chamber, while the ultra-thin layer of water with 6M KOH concentration is slightly warmer since the sample that is at a good thermal contact with the manipulator that is at room temperature of (~22 °C).

The only other detectable component within the electrolyte film is carbon. Under conditions within the meniscus film (6M KOH), the +1.05 V bias vs RHE results in a nearly zero potential difference between the meniscus film and the reference electrode. Based on the peak position for the sample biased at +1.05 V, this stems from adventitious carbon contamination (binding energy of 284.9 eV). This peak can be fitted with a single GL(30) function in CasaXPS with full-width half-maxima (FWHM) of 1.1 eV. Quantification of the carbon content shows a rather large value: for a thick electrolyte film, the ratio between C and O in the liquid film is 0.21 ± 0.05. This value is somewhat smaller for thinner films, with ratios of 0.12 for the 31 nm thick film and 0.06 for the 21 nm thick electrolyte film. Based on the C 1s peak position, this carbon contamination originates from an adventitious carbon and our future efforts will focus on reducing this contamination as much as possible. The C 1s peak position observed at a bias of +1.05 V also helps us to assign the O 1s peak located at 531 eV to hydroxyl radical groups (see middle panel of Fig. 6, black spectrum): while this peak could also be assigned to a signal from carbon containing oxygen groups such, as —C=O groups,[33] this assignment can be ruled out based on the measured C 1s binding energy.

The cyclic voltammogram (CV) shown in Fig. 7 was acquired *in situ* by means of our three electrode system and indicates the state of Ir(001) during the XPS measurements at +0.05 V and +1.05 V. The measurement was performed with a sample immersed inside the electrolyte, therefore, the CV is not affected by the lack of charge and mass transport within the thin meniscus film.[20] To the best of our knowledge, this is the first measured CV of a single-crystalline Ir(001) surface in 0.1M KOH. However, it is rather similar to the CV published in Ref. 34, which was also measured on Ir(001) and in an alkaline solution but in a different electrolyte at pH 11 (1 mM NaOH

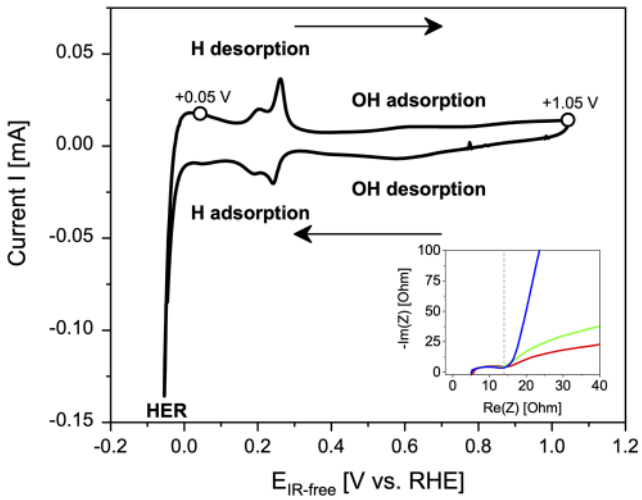

FIG. 7. Cyclic voltammogram of Ir(001) at 10 mV s^{-1} fully immersed in 0.1M KOH (after dip but before pull) measured before recording the XPS spectra shown in Fig. 6. The potentials are ohmic drop corrected (IR-free) and plotted on the RHE scale. The arrows indicate the direction of the potential scan. The inset shows the Nyquist plot of the three impedance spectroscopy measurements in the high frequency region at −0.05 V (red) at the beginning of the protocol, and at +0.05 V (green) and +1.05 V (blue) at the end of the protocol. The vertical dashed line at 14 Ω indicates the resistance used for the ohmic drop correction. (HER: hydrogen evolution reaction, Re: real part, Im: imaginary part, and Z: impedance.)

+ 0.1M $KClO_4$). The reductive peaks (negative current) measured between +0.3 V and 0.0 V are typical for the adsorption of hydrogen atoms from the electrolyte toward the surface of the WE.[34] The strong reductive current in the negative potential range is assigned to the hydrogen evolution reaction (HER). The oxidative peaks (positive current) measured between 0.0 V and +0.3 V are related to the desorption of the hydrogen atoms back into the electrolyte.[34] The small peak at +0.6 V is assigned to the hydroxide ion adsorption (positive current) and desorption (negative current) process.[34]

The Nyquist plot in the inset of Fig. 7 shows an ohmic resistance of 14 Ω. This low value indicates that the setup is suitable for electrochemical studies.

The *in situ* ambient pressure XPS measurements elucidated that Ir stays purely metallic at a potential of +0.05 V and +1.05 V when the potential during the CV was only cycled below +1.05 V. This is consistent with the findings in literature using alkaline solutions.[22]

A possible change of the Ir sample is the oxidation at higher potentials by forming a hydrous iridium oxide film (HIROF). Such oxidation is expected when the CV cycling reaches maximum potentials of around +1.5 V in alkaline solutions[35] as well as in acidic solutions.[36,37] This oxidation will lead then to growth of characteristic peaks at around +0.7 V, +1.0 V and +1.4 V in the CV which are related to different oxidation changes of the Ir.[35–37] The absence of those peaks in Fig. 7, as well as the Ir $4f_{7/2}$ core level peak position at 60.8 ± 0.1 eV[38] in Fig. 6, confirms the pure metallic state of bulk Ir electrode.

IV. CONCLUSIONS AND OUTLOOK

This new endstation is designed to serve a wide range of user communities in fields such as heterogeneous catalysis, battery research, photo(electro)chemistry, atmospheric chemistry, and corrosion science, to name a few. The endstation is designed to operate at two different beamlines at the SLS: a soft x-ray, bending magnet beamline (X07DB) and an undulator-type tender x-ray beamline PHOENIX I. The unique feature of this new setup lies in the possibility to prepare and characterize samples under UHV conditions, thus allowing us to study solid–liquid interfaces, or solid–gas interfaces at mbar-pressures, on model systems prepared under well-controlled conditions. While the presented results in this manuscript were performed outside equilibrium conditions (different temperatures and concentrations within the bulk electrolyte and the ultrathin electrolyte layer), later measurements performed on NiO the catalyst showed that this endstation can stabilize the ultrathin electrolyte layer of 0.1M KOH even at equilibrium conditions of 25 mbar of water vapor pressure (unpublished results). Therefore, this endstation is capable of probing systems with immediate relevance for the environment, such as studies of metal and metal oxides exposed to highly concentrated salts under equilibrium conditions. The versatility of this new endstation also comes from the fact that different manipulator inserts will be developed in the future, extending the range of experimental interfaces and systems that could be studied to areas such as gas–ice experiments, high temperature, and/or high-pressure oxidations of metals.

SUPPLEMENTARY MATERIAL

See the supplementary material for a description of our electrolyte outgassing setup and the experimental procedure.

ACKNOWLEDGMENTS

We would like to acknowledge Matthias Schreck and Martin Fischer from the Institut für Physik, Universität Augsburg, for providing single crystalline Ir(001) films used during commissioning of the endstation. The authors thank Marco Favaro and David Starr for fruitful discussions about the dip and pull technique, Blagoj Sarafimov for technical support, the Ferrovac team—Thomas Michlmayr, Stephan Michels, Marc Maier, and Claudio Weiss—for design and assembly of the endstation. This work was performed at the PHOENIX I (X07MB) beamline of the Swiss Light Source, Paul Scherrer Institut, Villigen PSI Switzerland. The new endstation has been financed by R'Equip Grant No. 206021_170747 of the Swiss National Science Foundation and with matching funds from the University of Zurich, the Paul Scherrer Institute, and the ETH Zurich. The University of Zurich Research Priority Program (URPP) LightChEC, and the Swiss National Science foundation (AP Energy Grant No. PYAPP2 160586) are gratefully acknowledged for financial support.

REFERENCES

[1] D. Frank Ogletree, H. Bluhm, E. D. Hebenstreit, and M. Salmeron, Nucl. Instrum. Methods Phys. Res., Sect. A **601**(1–2), 151–160 (2009).
[2] A. Knop-Gericke, E. Kleimenov, M. Hävecker, R. Blume, D. Teschner, S. Zafeiratos, R. Schlögl, V. I. Bukhtiyarov, V. V. Kaichev, I. P. Prosvirin, A. I. Nizovskii, H. Bluhm, A. Barinov, P. Dudin, and M. Kiskinova, in *Advances in Catalysis* (Academic Press, 2009), Vol. 52, pp. 213–272.
[3] M. Salmeron and R. Schlögl, Surf. Sci. Rep. **63**(4), 169–199 (2008).
[4] D. E. Starr, Z. Liu, M. Havecker, A. Knop-Gericke, and H. Bluhm, Chem. Soc. Rev. **42**(13), 5833–5857 (2013).
[5] H. Bluhm, M. Hävecker, A. Knop-Gericke, M. Kiskinova, R. Schlögl, and M. Salmeron, MRS Bull. **32**(12), 1022–1030 (2007).
[6] D. F. Ogletree, H. Bluhm, G. Lebedev, C. S. Fadley, Z. Hussain, and M. Salmeron, Rev. Sci. Instrum. **73**(11), 3872–3877 (2002).
[7] J. Cai, Q. Dong, Y. Han, B.-H. Mao, H. Zhang, P. G. Karlsson, J. Åhlund, R.-Z. Tai, Y. Yu, and Z. Liu, Nucl. Sci. Tech. **30**(5), 81 (2019).
[8] S. G. Booth, A. M. Tripathi, I. Strashnov, R. A. W. Dryfe, and A. S. Walton, J. Phys.: Condens. Matter **29**(45), 454001 (2017).
[9] O. Björneholm, M. H. Hansen, A. Hodgson, L.-M. Liu, D. T. Limmer, A. Michaelides, P. Pedevilla, J. Rossmeisl, H. Shen, G. Tocci, E. Tyrode, M.-M. Walz, J. Werner, and H. Bluhm, Chem. Rev. **116**(13), 7698–7726 (2016).
[10] H. Bluhm, J. Electron Spectrosc. Relat. Phenom. **177**(2), 71–84 (2010).
[11] C. Escudero and M. Salmeron, Surf. Sci. **607** (Suppl. C), 2–9 (2013).
[12] M. A. Brown, A. B. Redondo, I. Jordan, N. Duyckaerts, M. T. Lee, M. Ammann, F. Nolting, A. Kleibert, T. Huthwelker, J. P. Machler, M. Birrer, J. Honegger, R. Wetter, H. J. Worner, and J. A. van Bokhoven, Rev. Sci. Instrum. **84**(7), 8 (2013).
[13] H. S. Casalongue, S. Kaya, V. Viswanathan, D. J. Miller, D. Friebel, H. A. Hansen, J. K. Nørskov, A. Nilsson, and H. Ogasawara, Nat. Commun. **4**(1), 2817 (2013).
[14] V. Streibel, M. Hävecker, Y. Yi, J. J. Velasco Vélez, K. Skorupska, E. Stotz, A. Knop-Gericke, R. Schlögl, and R. Arrigo, Top. Catal. **61**(20), 2064–2084 (2018).
[15] T. Zubkov, D. Stahl, T. L. Thompson, D. Panayotov, O. Diwald, and J. T. Yates, J. Phys. Chem. B **109**(32), 15454–15462 (2005).
[16] J. Knudsen, J. N. Andersen, and J. Schnadt, Surf. Sci. **646**, 160–169 (2016).
[17] S. Axnanda, E. J. Crumlin, B. H. Mao, S. Rani, R. Chang, P. G. Karlsson, M. O. M. Edwards, M. Lundqvist, R. Moberg, P. Ross, Z. Hussain, and Z. Liu, Sci. Rep. **5**, 12 (2015).
[18] M. Favaro, B. Jeong, P. N. Ross, J. Yano, Z. Hussain, Z. Liu, and E. J. Crumlin, Nat. Commun. **7**, 12695 (2016).
[19] M. Favaro, J. Yang, S. Nappini, E. Magnano, F. M. Toma, E. J. Crumlin, J. Yano, and I. D. Sharp, J. Am. Chem. Soc. **139**(26), 8960–8970 (2017).

[20]O. Karslioglu, S. Nemsak, I. Zegkinoglou, A. Shavorskiy, M. Hartl, F. Salmassi, E. M. Gullikson, M. L. Ng, C. Rameshan, B. Rude, D. Bianculli, A. A. Cordones, S. Axnanda, E. J. Crumlin, P. N. Ross, C. M. Schneider, Z. Hussain, Z. Liu, C. S. Fadley, and H. Bluhm, Faraday Discuss. **180**, 35–53 (2015).
[21]M. F. Lichterman, S. Hu, M. H. Richter, E. J. Crumlin, S. Axnanda, M. Favaro, W. Drisdell, Z. Hussain, T. Mayer, B. S. Brunschwig, N. S. Lewis, Z. Liu, and H.-J. Lewerenz, Energy Environ. Sci. **8**(8), 2409–2416 (2015).
[22]M. F. Lichterman, M. H. Richter, B. S. Brunschwig, N. S. Lewis, and H.-J. Lewerenz, J. Electron Spectrosc. Relat. Phenom. **221**, 99–105 (2017).
[23]D. E. Starr, M. Favaro, F. F. Abdi, H. Bluhm, E. J. Crumlin, and R. van de Krol, J. Electron Spectrosc. Relat. Phenom. **221**, 106–115 (2017).
[24]F. Orlando, A. Waldner, T. Bartels-Rausch, M. Birrer, S. Kato, M.-T. Lee, C. Proff, T. Huthwelker, A. Kleibert, J. van Bokhoven, and M. Ammann, Top. Catal. **59**(5-7), 591–604 (2016).
[25]J. Raabe, G. Tzvetkov, U. Flechsig, M. Böge, A. Jaggi, B. Sarafimov, M. G. C. Vernooij, T. Huthwelker, H. Ade, D. Kilcoyne, T. Tyliszczak, R. H. Fink, and C. Quitmann, Rev. Sci. Instrum. **79**(11), 113704 (2008).
[26]H. Cun, A. Spescha, A. Schuler, M. Hengsberger, J. Osterwalder, and T. Greber, J. Vac. Sci. Technol., A **34**(2), 020602 (2016).
[27]H. Shinotsuka, B. Da, S. Tanuma, H. Yoshikawa, C. J. Powell, and D. R. Penn, Surf. Interface Anal. **49**(4), 238–252 (2017).
[28]M. B. Trzhaskovskaya and V. G. Yarzhemsky, At. Data Nucl. Data Tables **119**, 99–174 (2018).
[29]M. E. Grass, P. G. Karlsson, F. Aksoy, M. Lundqvist, B. Wannberg, B. S. Mun, Z. Hussain, and Z. Liu, Rev. Sci. Instrum. **81**(5), 7 (2010).
[30]W. M. Haynes, D. R. Lide, and T. J. Bruno, *CRC Handbook of Chemistry and Physics* (CRC Press, 2019).
[31]P. Novotný and O. Söhnel, J. Chem. Eng. Data **33**(1), 49–55 (1988).
[32]J. Balej, Int. J. Hydrogen Energy **10**(4), 233–243 (1985).
[33]M. Lampimäki, S. Schreiber, V. Zelenay, A. Křepelová, M. Birrer, S. Axnanda, B. Mao, Z. Liu, H. Bluhm, and M. Ammann, J. Phys. Chem. C **119**(13), 7076–7085 (2015).
[34]T. Pajkossy, L. A. Kibler, and D. M. Kolb, J. Electroanal. Chem. **600**(1), 113–118 (2007).
[35]L. D. Burke and R. A. Scannell, J. Electroanal. Chem. Interfacial Electrochem. **175**(1), 119–141 (1984).
[36]S. Geiger, O. Kasian, B. R. Shrestha, A. M. Mingers, K. J. J. Mayrhofer, and S. Cherevko, J. Electrochem. Soc. **163**(11), F3132–F3138 (2016).
[37]D. N. Buckley and L. D. Burke, J. Chem. Soc., Faraday Trans. 1 **71**, 1447–1459 (1975).
[38]S. J. Freakley, J. Ruiz-Esquius, and D. J. Morgan, Surf. Interface Anal. **49**(8), 794–799 (2017).